THE JOURNAL OF PHYSICAL CHEMISTRY C

ARTICLE

pubs.acs.org/JPCC

Full Compositional Flexibility in the Preparation of Mesoporous MFI Zeolites by Desilication

Danny Verboekend,[†] Sharon Mitchell,[†] Maria Milina,[†] Johan C. Groen,[‡] and Javier Pérez-Ramírez*[,†]

[†]Institute for Chemical and Bioengineering, Department of Chemistry and Applied Biosciences, ETH Zurich, Wolfgang-Pauli-Strasse 10, HCI E 125, CH-8093, Zurich, Switzerland

[‡]Delft Solids Solutions B.V., Rotterdamseweg 183c, 2629 HD Delft, The Netherlands

Supporting Information

ABSTRACT: We demonstrate that desilication in alkaline medium is a suitable post-synthetic method to introduce intracrystalline mesoporosity in MFI zeolites independent of the Si/Al ratio in the parent material. By systematic screening of the influence of both base concentration (0.1−1.8 M NaOH) and Si/Al ratio (10−1000) on the properties of the treated zeolites, we reveal that effective mesoporosity introduction (>200 m^2 g^{-1}) may be achieved in the Si/Al range of 12−200. The use of descriptors like the "indexed hierarchy factor" and the "desilication efficiency" enable the rational categorization of the solids obtained. The highest desilication efficiencies, estimated by correlating the introduced mesoporosity with the yields after NaOH treatment, are obtained in the previously established Si/Al range of 25−50. We identify the crucial role of a subsequent acid treatment for removing amorphous Al-rich debris from alkaline-treated samples in the case of low Si/Al ratios (<20). The latter acid wash uncovers the complete micro- and mesopore network, enabling full compositional flexibility of desilication. The removal of these debris concomitantly enabled restoration of both the acidity and the chemical composition of the hierarchical zeolite to that of the starting (purely microporous) zeolite. Catalytic evaluation of selected Al-rich zeolites in the alkylation of toluene with benzyl alcohol, confirmed the superiority of the mesoporous alkaline-treated samples with respect to the parent material. Hierarchical ZSM-5 after acid washing stands as the most active sample, which stresses the relevance of the additional post-synthetic treatment step.

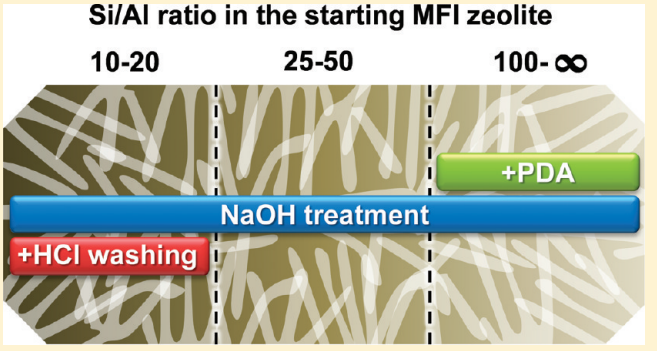

1. INTRODUCTION

The promising properties of hierarchical (mesoporous) zeolites, i.e., those combining the intrinsic microporosity with an auxiliary network of mesopores, have sparked intense effort to improve the zeolite utilization in catalysis.[1−4] Among the numerous methods available to prepare mesoporous zeolites, desilication by alkaline treatment is one of the most widely applied, established as a simple and effective approach.[5,6] Furthermore, the increasing number of zeolite families, prepared in hierarchical form by alkaline treatment (MFI,[7] MTW,[8] MOR,[9] BEA,[10] AST,[11] FER,[12] MWW,[13] IFR,[14] STF,[15] CHA,[16] FAU,[17] and TON[18]) highlights its versatility.

Pioneering work on desilication was performed by Groen et al.,[19,20] who identified, by applying NaOH treatment on MFI zeolites at a fixed condition, that a confined molar framework Si/Al window (25−50) for optimal intracrystalline mesopore formation exists. At higher Si/Al ratios, uncontrolled silicon extraction occurs, resulting in the formation of larger pores. For low Si/Al ratios, silicon extraction is hampered resulting in limited extra mesoporosity. Consequently, framework aluminum was coined as "pore-directing agent" (PDA), due to its regulatory effect on silicon leaching. Apart from Al^{3+}, other trivalent heteroatoms in lattice positions (Fe^{3+}, Ga^{3+}, B^{3+}) also proved successful in exerting the role of PDA.[21] Several routes to tune the desilication process over zeolites within the optimal range of Si/Al ratios have been reported, e.g., partial detemplation−desilication,[22] the application of microwave irradiation,[23] and the use of alternative bases[24,25] or pore-growth moderators.[26] Additionally, by combining alkaline with steam[27] or acid[28] treatments, the mesopore formation was decoupled from acidity modification.

Apart from optimization of the desilication treatment, significant progress concerning the in-depth characterization and categorization of hierarchical zeolites has been achieved. For example, the accessibility index (ACI)[29] provides a powerful tool to standardize acid site accessibility in zeolites, while the hierarchy factor (HF)[26] couples the developed mesoporosity to the preserved intrinsic microporosity. More specifically for alkaline leaching, the "desilication efficiency" was recently introduced in

Received: February 20, 2011
Revised: June 9, 2011
Published: June 13, 2011

consideration of the zeolite weight loss incurred upon introduction of mesoporosity.[18]

An important advance in the preparation of mesoporous all-silica zeolites by desilication was the use of external PDAs, such as tetraalkylammonium cations or metal complexes. The deliberate addition of PDAs to the alkaline solution enabled the preparation of mesoporous silicalite-1.[30] In addition to expanding the range of feasible Si/Al ratios to infinity, this work demonstrated that the pore-directing action is executed at the external surface of the zeolite. The latter implies that framework aluminum (or any other trivalent cation) does not play a direct pore-directing role. Instead, only aluminum extracted from the framework actively participates in pore formation, by an "alkaline-induced alumination" of the crystals' external surface. In conclusion, three major factors were identified to govern the formation of intracrystalline mesoporosity: (i) the zeolite, (ii) the treatment conditions, and (iii) the presence of PDAs.

The final hurdle to achieve full compositional flexibility in the preparation of mesoporous zeolites by desilication requires tackling the low Si/Al range. To date, mesoporous Al-rich MFI zeolites are mostly prepared via a different approach, e.g., by carbon templating[31] or by altering the composition to within the optimal window by dealumination prior to alkaline treatment.[32] However, in the latter case, the mesoporous zeolite no longer comprises an Al-rich framework. Strikingly, although the literature suggests that alkalinity is of critical importance,[8] the impact of base concentration on mesoporosity development in low Si/Al ratio zeolites has not been systematically explored. Previous studies with varying alkalinity have primarily focused on individual zeolites of Si/Al ratios within or near the preferred range (25−50), adjusting to either framework structure or morphology.[7,12,19,33−36]

Herein, we provide further insight into the mechanism of mesopore formation in basic media enabling full compositional flexibility in the preparation of hierarchical zeolites. Exploring the entire range of Si/Al ratios in MFI (10−1000), we probe the influence of base concentration on the properties of the treated zeolites. By monitoring changes in yield, crystallinity, and porosity, we map the formation of mesoporous zeolites enabling their purpose design. Descriptors as the indexed hierarchy factor and the desilication efficiency are used to categorize the porous structures obtained and to relate the mesoporosity developed with the associated weight loss. We show that mesoporous Al-rich zeolites can be prepared by desilication at high base concentrations, leading to an improved performance in toluene alkylation with benzyl alcohol. However, a subsequent acid treatment of the alkaline-treated samples is of paramount importance to remove amorphous Al-rich debris thereby uncovering the entire micro- and mesopore network. Moreover, the acid treatment enables restoration of both the Si/Al ratio and the acidity and further enhances the catalytic activity.

2. EXPERIMENTAL SECTION

2.1. Post-synthetic Treatments. Various commercial MFI zeolites in ammonium form were used in the post-synthetic treatments: Z10 (PZ2/23, Zeochem), Z15 (CBV 3024E, Zeolyst International), Z25 (CBV 5524G, Zeolyst International), Z40 (CBV 8014, Zeolyst International), and Z1000 (HSZ-890H0A, Tosoh Corporation). The number in the Z*x* code refers to the Si/Al ratio according to the manufacturer's specifications. The parent zeolites (code P) were obtained by calcination of the as-received powders by heating to 823 K at 5 K min^{-1} and thermal treatment for 5 h in static air. Alkaline treatments were carried out in 0.1−1.8 M aqueous NaOH (3.3 g of zeolite per 100 cm^3 of solution) using an Easymax™ 102 reactor system from Mettler Toledo. In a typical experiment, the alkaline solution was stirred at 500 rpm and heated to 338 K, after which the parent zeolite sample was introduced. The resulting suspension was left to react for 30 min, followed by quenching, filtration, extensive washing using distilled water, and overnight drying at 338 K. Some samples were subsequently acid treated in 0.02−0.1 M aqueous HCl (1 g zeolite per 100 cm^3 of solution) at 338 K for 6 h. Prior to acidity characterization and catalytic testing, the zeolites were converted into the protonic form by three consecutive ion exchanges in 0.1 M aqueous NH_4NO_3 (298 K, 12 h, 1 g zeolite per 100 cm^3 of solution), followed by calcination as described for the parent zeolite. Treated samples were coded "*x*NaOH" or "*y*HCl", where *x* and *y* represent the molarity of the NaOH and HCl solutions, respectively. Yields were corrected for loss through handling (10%), which was determined by reproducing the treatments using distilled water.

2.2. Characterization. N_2 isotherms were measured in a Quantachrome Quadrasorb-SI gas adsorption analyzer at 77 K. Samples were degassed in vacuum at 573 K for 10 h prior to measurement. The total pore volume was derived from the amount of N_2 adsorbed at $p/p_0 = 0.99$, and the *t*-plot method[37] was used to discriminate between micro- and mesoporosity. The Brunauer−Emmett−Teller (BET) method[38] was applied to determine the total surface area (S_{BET}), which is used for comparative purposes. The mesopore size distribution was obtained by applying the Barrett−Joyner−Halenda (BJH) method[39] to the adsorption branch of the isotherm.

X-ray diffraction (XRD) was undertaken using a PANalytical X'Pert PRO-MPD diffractometer equipped with Bragg−Brentano geometry and Ni-filtered Cu Kα radiation ($\lambda = 0.1541$ nm). Data were recorded in the range of 5−50° 2θ, with an angular step size of 0.05° and a counting time of 8 s per step. Samples were ground to minimize the effects of preferred orientation and supported on a flat specimen holder, with a fixed sample volume irradiated by the X-ray beam. The variation in zeolite crystallinity resulting from post-synthetic modification was derived from the relative intensity of the intense (051) reflection at 23° 2θ, assuming 100% crystallinity in the parent sample. The reproducibility of the crystallinity analysis was within 1%.

The Si and Al content in selected solids and filtrates collected after alkaline and acid treatments were analyzed by atomic absorption spectroscopy (AAS) in a Varian SpectrAA 220 FS spectrometer.

Transmission electron microscopy (TEM) imaging was performed with a Phillips CM12 instrument operated at 100 kV.

Magic angle spinning nuclear magnetic resonance (MAS NMR) spectra were recorded at a spinning speed of 8 kHz on a Bruker Avance 700 NMR spectrometer equipped with a 4 mm probe head and 4 mm ZrO_2 rotors at 182.4 MHz. ^{27}Al spectra were recorded using 2048 accumulations, 90° pulses with a pulse length of 2.4 μs, a recycle delay of 0.25 s, and $(NH_4)Al(SO_4)_2 \cdot 12H_2O$ as the reference. ^{29}Si spectra were acquired using 2048 accumulations, 90° pulses with a pulse length of 12.5 μs, a recycle delay of 10 s, and 2,2-dimethyl-2-silapentane-5-sulfonic acid as the reference.

Infrared spectroscopy was performed under a N_2 atmosphere at 473 K using a Thermo Nicolet 5700 spectrometer equipped with a SpectraTech Collector II diffuse reflectance accessory and a high-temperature cell. Prior to the measurement, the sample was dried at 573 K in N_2 flow (100 cm^3 min^{-1}) for 60 min.

Spectra were recorded in the range of 650−4000 cm^{-1} with a nominal resolution of 4 cm^{-1} and coaddition of 200 scans.

Temperature-programmed desorption of ammonia (NH_3-TPD) was carried out in a Thermo TPDRO 1100 unit equipped with a thermal conductivity detector. The zeolite (100 mg) was pretreated at 823 K in He flow (20 cm^3 min^{-1}) for 2 h. Afterwards, 10 vol % NH_3 in He (20 cm^3 min^{-1}) was adsorbed at 473 K for 30 min followed by He purging at the same temperature for 1 h. This procedure was repeated three times. Desorption of NH_3 was monitored in the range of 473−973 K using a ramp rate of 10 K min^{-1}.

2.3. Catalytic Measurements. The alkylation of toluene with benzyl alcohol was conducted in an Endeavor Catalyst Screening System (Argonaut Technologies), consisting of eight parallel reactors with a working volume of 5 cm^3 and with continuous stirring by overhead impellers. Reaction conditions were P = 0.5 MPa, T = 433 K, molar toluene-to-benzyl alcohol ratio (T/BA) = 80, and catalyst amount = 40 wt % of zeolite with respect to the amount of benzyl alcohol. Liquid samples were analyzed at different reaction times using a gas chromatograph (HP 6890) coupled to a mass selective detector (HP 5973).

3. RESULTS AND DISCUSSION

3.1. Two-Dimensional Screening of Desilication. Alkaline treatments were performed over various commercial MFI zeolites representative of the full Si/Al range for MFI, i.e., Z10, Z15, Z25, Z40, and Z1000. ^{27}Al MAS NMR evidenced that the parent zeolites contained predominantly tetrahedral Al (band at 59 ppm), ascribed to aluminum in framework positions (Figure SI1). Additionally, some octahedrally coordinated Al (band at 0 ppm), attributed to extra-framework aluminum, was demonstrated. The contribution of the latter species decreased with the Si/Al ratio; in the case of Z10 a significant amount was present; for Z15 and Z25 minor amounts were evidenced, whereas for Z40 and Z1000 no distinguishable contributions appeared. The influence of the extra-framework aluminum in the case of Z10 is discussed in section 3.2. The temperature (338 K) and time (30 min) of the alkaline treatments were kept constant, while the NaOH concentration was varied between 0.1 and 1.8 M. In Figure 1 selected nitrogen isotherms and corresponding BJH mesopore size distributions illustrate the porous properties of the parent and treated zeolites. Table SI1 provides a complete overview of parent and treated zeolites. In Figure 2, various contour plots illustrate the variation in yield, crystallinity, and porous properties of the solids derived from the two-dimensional screening. Additionally, two contour plots concern the indexed hierarchy factor, which is explained below.

Yield, Crystallinity, and Porosity. Figure 2a shows that, in line with Čižmek et al.,[40] yields reduced with increasing NaOH concentration and Si/Al ratio of the parent zeolite. The yields for Z40 and Z1000 did not differ much due to the relative abundance of Si. On the other hand, for Si/Al < 25, the changes in yields were more pronounced. For example, to obtain a yield of ca. 60%, Z15 required an alkalinity substantially higher (0.7 M NaOH) than that for Z25 (0.4 M NaOH). Since upon alkaline treatment, intracrystalline mesopores are formed by selective dissolution, a reduced yield (typically ca. 60−70%) is a prerequisite to obtain substantial mesopore surface areas.[18,30] We can therefore deduce that, in order to create intracrystalline mesopores in zeolites of Si/Al ratio <20, an increased alkalinity is required.

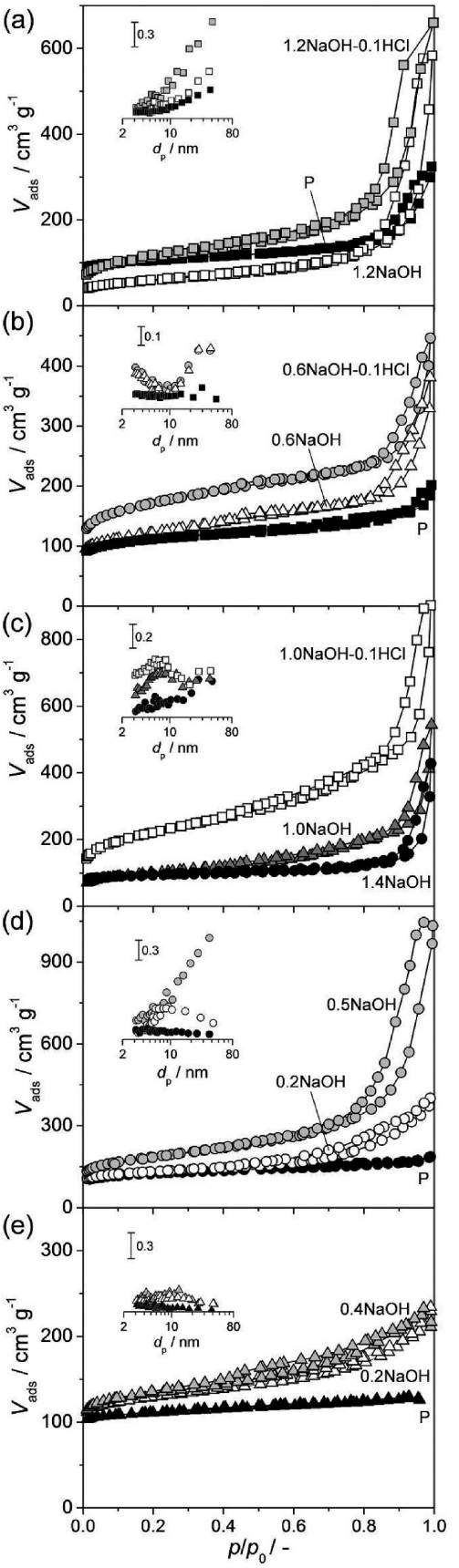

Figure 1. N_2 isotherms of parent and treated Z10 (a), Z15 (b, c) Z40 (d), and Z1000 (e) zeolites. The insets represent the BJH mesopore size distributions.

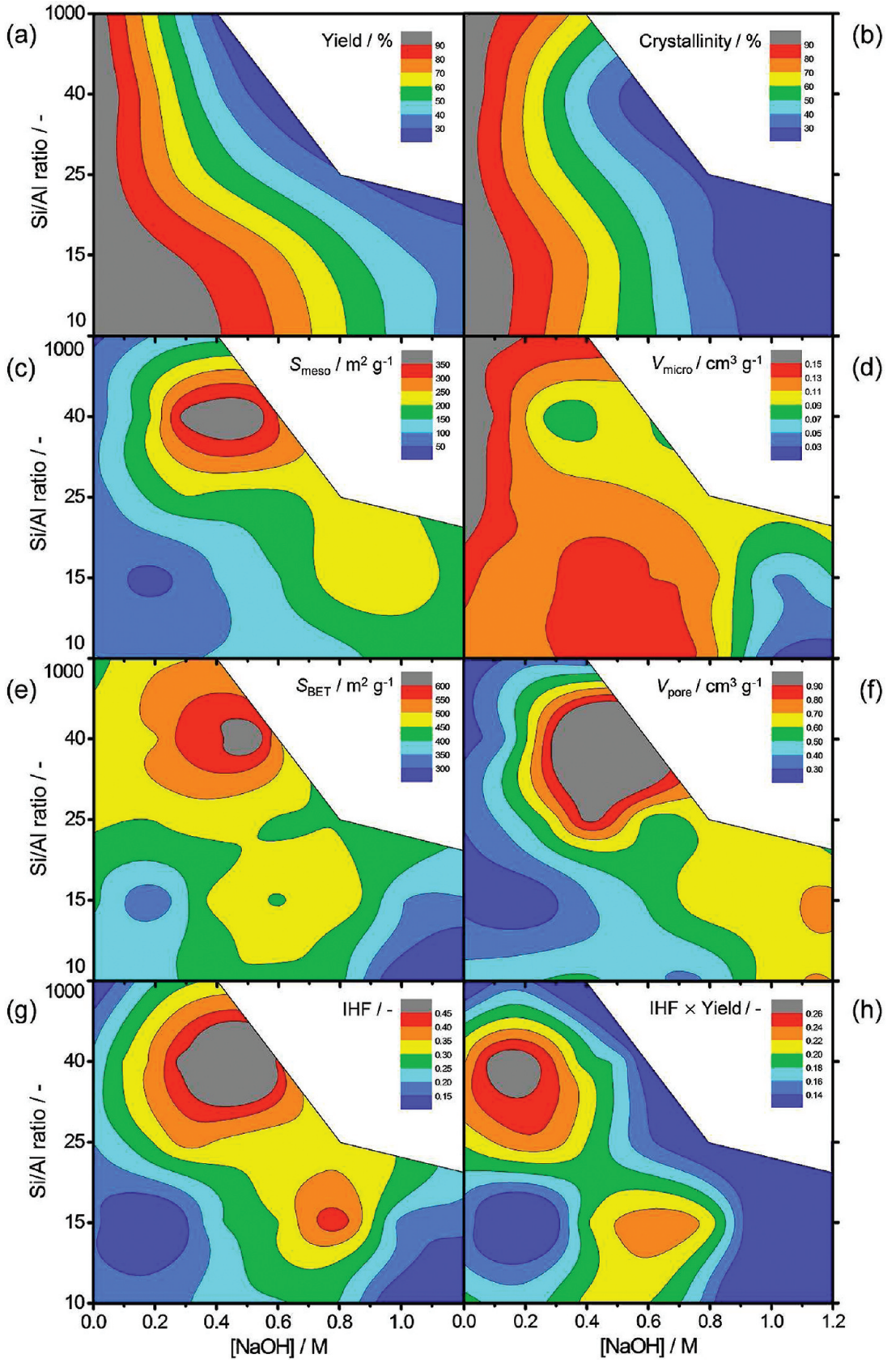

Figure 2. Contour plots obtained by alkaline treatments performed on MFI zeolites, as a function of the bulk Si/Al ratio of the parent samples (*y*-axis) and concentration of NaOH (*x*-axis). The influence of the zeolite composition and alkalinity on the yield (a), crystallinity (b), S_{meso} (c), V_{micro} (d), S_{BET} (e), V_{pore} (f), indexed hierarchy factor (IHF) (g), and IHF multiplied by yield (h) is shown.

dx.doi.org/10.1021/jp201671s |*J. Phys. Chem. C* 2011, 115, 14193–14203

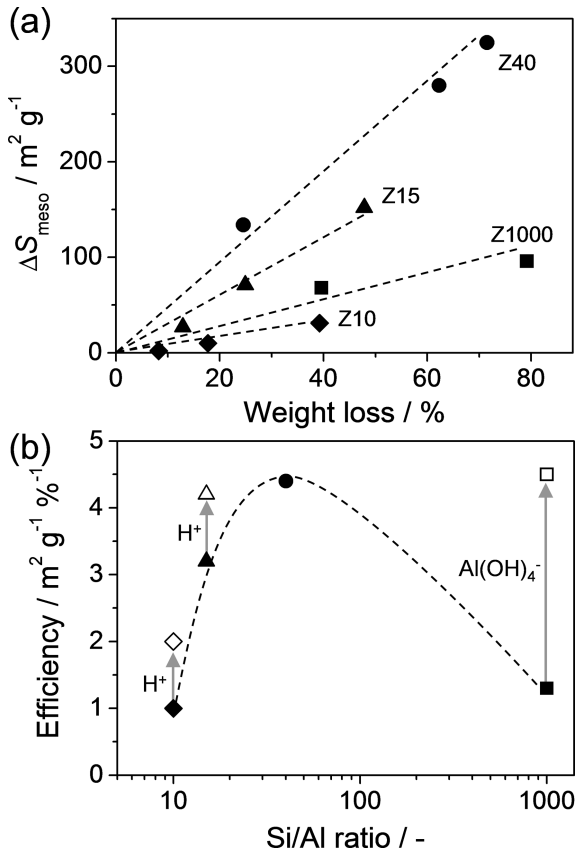

Figure 3. Linear relationship between the increase in introduced mesopore surface area ($\Delta S_{meso} = S_{meso,AT} - S_{meso,P}$) and the weight loss upon desilication of ZSM-5 zeolites with framework Si/Al ratios in the range 10−1000 (a). The slopes of the linear trends represent the desilication efficiency (m^2 g^{-1} $\%^{-1}$). Variation in desilication efficiency with respect to the Si/Al ratio of the parent zeolite (b). The desilication efficiency of conventional alkaline treatment (solid symbols) is highest for zeolites with Si/Al ratio = 25−50. Open symbols indicate the increased desilication efficiency due to either subsequent acid washing H^+ for Al-rich zeolites (this work) or the use of $Al(OH)_4^-$ as external pore-directing agent in the case of all-silica zeolites.[30]

Substantial mesopore surfaces areas ($S_{meso} \geq 200$ m^2 g^{-1}) were measured for virtually all MFI zeolites studied, emphasizing the wide compositional flexibility of desilication (Figure 2c). The highest values (>300 m^2 g^{-1}) were obtained for Z40, whereas the lowest surface areas were obtained at the extremes of the MFI Si/Al spectrum, that is, for Z1000 (maximum 132 m^2 g^{-1}) and Z10 (maximum 170 m^2 g^{-1}). Consequently, the range in which alkaline treatment (using only aqueous NaOH) is able to introduce significant mesoporosity in MFI zeolites is much broader (ca.12−200) than that initially established (25−50).[20] The latter limit appears to be suitable mostly for conditions similar to the "standard" alkaline treatment (0.2 M NaOH, 65 °C, 30 min, zeolite-to-liquid ratio = 33 g L^{-1}). For low Si/Al ratios, the highest external surface areas are achieved at higher NaOH concentrations, in agreement with the results from Figure 2a.

Figure 2b shows that the greatest loss of crystallinity occurs for the most mesoporous samples (e.g., Z40 treated in 0.5 M NaOH), as well as for the zeolites of Si/Al < 25 treated in NaOH concentrations exceeding 0.6 M. The relatively small crystallinity loss for Z1000 should be related to the absence of substantial mesoporosity, while the strong crystallinity decrease upon desilication of zeolites of low Si/Al ratio exposed to high alkaline concentrations is assigned to the presence of both intracrystalline mesopores and amorphous debris (vide infra).

A decrease of the micropore volume (V_{micro}) is frequently observed upon NaOH treatment of zeolites.[14,17,18,20,26] Figure 2d shows that this reduction increases with the Al content of the parent zeolite. In the case of Z1000, the reduction of V_{micro} is limited (down to 0.13 cm^3 g^{-1}), despite extensive dissolution. For Z40 the reduction is more pronounced; especially the more mesoporous samples (S_{meso} > 300 m^2 g^{-1}) display significantly reduced micropore volumes (down to ca. 0.10 cm^3 g^{-1}). A severe reduction of V_{micro} (down to ca. 0.03 cm^3 g^{-1}) is observed for zeolites with Si/Al < 15 treated at NaOH concentrations greater than 0.8 M. In line with previous observations,[18,41] this suggests that the micropore reduction is due to the presence of amorphous Al-rich debris.

The variations in S_{meso} and V_{micro} are directly reflected in the BET surface area. Figure 2e shows that the maximum corresponds reasonably to the maximum obtained for the developed S_{meso} (obtained for Z40, treated in 0.5 M NaOH). On the other hand, S_{BET} decreases strongly upon reduction of the micropore volume (Si/Al < 15, alkalinity > 0.8 M NaOH). Hence, from the total surface area alone one can already get an indication of the quality of hierarchical pore systems. Since ideally the introduced auxiliary porosity is coupled to a fully preserved microporosity, the total surface area in a superior hierarchical zeolite should be higher than that of its purely microporous analogue.

The total pore volume (V_{pore}) increases with the alkalinity for all zeolites due to the introduction of mesopores (Figure 2f). Similar to the trend in yield and S_{meso}, the highest values are obtained for Si/Al = 40, and Si/Al ratios <25 require higher alkalinities to obtain an increased V_{pore}. For the latter Si/Al range, the maximum total pore volumes are obtained at ca. 0.2 M higher molarities compared to the maximum in S_{meso}. This should be due to the greater contribution of large mesopores and macropores to the pore volume than to the external surface.

Indexed Hierarchy Factor. As said earlier, the introduction of mesoporosity in zeolites is frequently coupled to a reduction of the micropore volume. With this in mind, the hierarchy factor (HF) was introduced, relating a relative mesoporosity (S_{meso}/S_{BET}) to a relative microporosity (V_{micro}/V_{pore}). This factor proved to be very helpful in rationalizing the entire field of mesoporous zeolites, in particular with respect to the different framework types and preparative approaches. Moreover, relation of the hierarchy factor of mesoporous zeolites with catalytic activity yielded sensible trends in alkylation and pyrolysis reactions.[14,26] Herein, we introduce a variation of the hierarchy factor that fulfills the same function, but is more sensitive to the method applied and the framework type. The micropore volume of MFI is known (ca. 0.16 cm^3 g^{-1}), and the maximum amount of mesopore surface area obtained by desilication can be derived from our screening (403 m^2 g^{-1}, see Table SI1). We can therefore normalize both V_{micro} and S_{meso} with respect to their maximum values, i.e., IHF = $(V_{micro}/V_{micro,max}) \times (S_{meso}/S_{meso,max})$. Since the obtained values are normalized (in this case to MFI and desilication), we have coined this modified version as the "indexed hierarchy factor". Figure 2g shows the indexed hierarchy factor (IHF) as a function of Si/Al ratio and NaOH concentration. The IHF is optimal in the region of highest mesoporosity development (Si/Al = 40, 0.5 M NaOH). In fact, the contour plot follows closely the pattern of S_{meso}. The only noticeable difference comprises Si/Al < 15 treated at

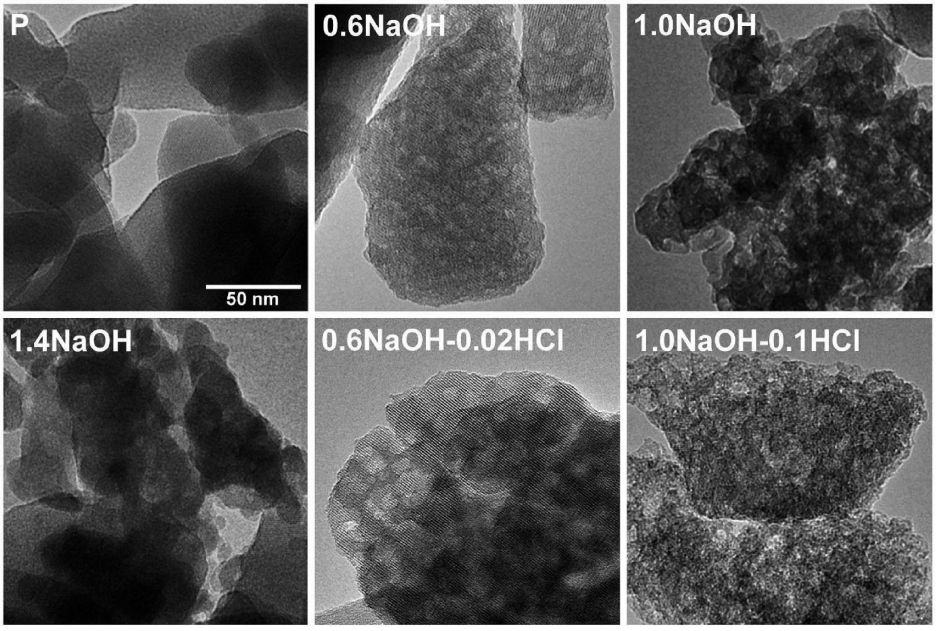

Figure 4. TEM images of parent and treated Z15 zeolites. The same scale bar applies to all the micrographs.

concentrations of 0.9−1.2 M; in this area the remarkable drop in microporosity leads to lower values. When the IHF is extended to take into account the zeolite loss, by factoring the IHF by the yield,

a similar pattern is observed, but shifted to lower NaOH concentrations (Figure 2h). The shift is more pronounced for zeolites with Si/Al > 40, due to the sharp dependence of the yield on the alkalinity. The importance of the yield is further illustrated below.

Desilication Efficiency. With an open eye to industrialization, we examine the degree of zeolite dissolution upon introducing external surface area in more detail. The descriptor "desilication efficiency" was recently developed, relating the increase in mesopore surface area to the weight loss upon desilication.[18] Figure 3a shows the increase in mesopore surface area (ΔS_{meso}) plotted against the weight loss upon alkaline treatment of Z10, Z15, Z40, and Z1000. It should be noted that the external surface area present in the parent sample is typically derived from mostly intercrystalline mesopores, whereas the alkaline-treated samples comprise mostly intracrystalline mesopores. This suggests that, in some cases, the ΔS_{meso} may underestimate the introduced intracrystalline mesopore surface area. The data points in Figure 3a correspond to zeolites treated with 0.1−1.0 M NaOH. A linear correlation is observed in all cases, albeit with a different slope. This slope ($dS_{meso}/d(\text{weight loss})$) is defined as the desilication efficiency and depends strongly on the Si/Al ratio of the starting zeolite. In the case of Z40 the mesopore surface increased by ca. 4.5 $m^2\ g^{-1}$ per percentage of weight loss (hereafter $m^2\ g^{-1}\ \%^{-1}$). Concerning Z15, the mesopore surface area increased by ca. 3 $m^2\ g^{-1}\ \%^{-1}$. For Z10 and Z1000 the desilication efficiency was limited to ca. 1 $m^2\ g^{-1}\ \%^{-1}$. Figure 3b compares the desilication efficiencies with respect to the Si/Al ratio of the parent zeolites, resulting in a volcano plot centered around Si/Al = 40. Hence, from Figure 3 we conclude that the preparation of hierarchical zeolites by alkaline treatment is (i) most effective (largest external surface) and (ii) most efficient (smallest relative weight loss) for zeolites with Si/Al ratio in the range of 25−50. The lower desilication efficiencies obtained at the extremes of the compositional Si/Al spectrum are attributed to differences in the mechanism of zeolite dissolution. In the absence of Al (Z1000), the development is mesoporosity is hampered due to the more unselective dissolution. In the case of zeolites with low Si/Al ratio (Z10, Z15), a reduced efficiency arises due to the impeding effect of Al-rich debris. The latter aspect is detailed in section 3.2.

3.2. Desilication of Low Si/Al Ratio MFI Zeolites. *Introduction of Mesoporosity by Alkaline Treatment.* Desilication aimed at introducing mesoporosity in MFI zeolites with low Si/Al ratio zeolites is relatively unexplored. This study investigates the introduction of mesoporosity in these zeolites using alkaline solutions of increasing NaOH concentration. We focused particularly on the preparation of mesoporous Z15.

N_2 adsorption performed on the parent Z15 resulted in a type I isotherm characteristic of conventional mostly microporous zeolites (Figures 1b, c). Not uncommon to commercial zeolites, the parent material revealed a considerable S_{meso} (76 $m^2\ g^{-1}$, Table SI1). The BJH mesopore distribution did not show intracrystalline mesopores, and TEM (Figure 4) confirmed that the external surface area is attributable to intercrystalline voids. Additionally, a micropore volume of 0.14 $cm^3\ g^{-1}$ was evidenced.

Upon contacting the parent with solutions of increasing alkalinity, yields gradually decreased (down to 20% at 1.8 M NaOH), indicating a more extensive zeolite dissolution (Figure 5a). In line with the high Al content in the parent zeolite, the filtrate collected after treatment with 1.0 M NaOH evidenced a relatively low Si/Al ratio (89, Table 1). The preferential removal of silicon reduced the Si/Al ratio of the solid to 3 (1.0NaOH). Also 1.4 NaOH, which displayed a similar weight loss upon alkaline treatment, comprised a Si/Al ratio of 3.

In agreement with the mesopore surface areas observed in Figure 2c, increased uptakes at middle-to-high relative pressures were seen for the treated Z15 samples 0.6NaOH and 1.0NaOH (Figure 1b, c). The external surface areas accounted to

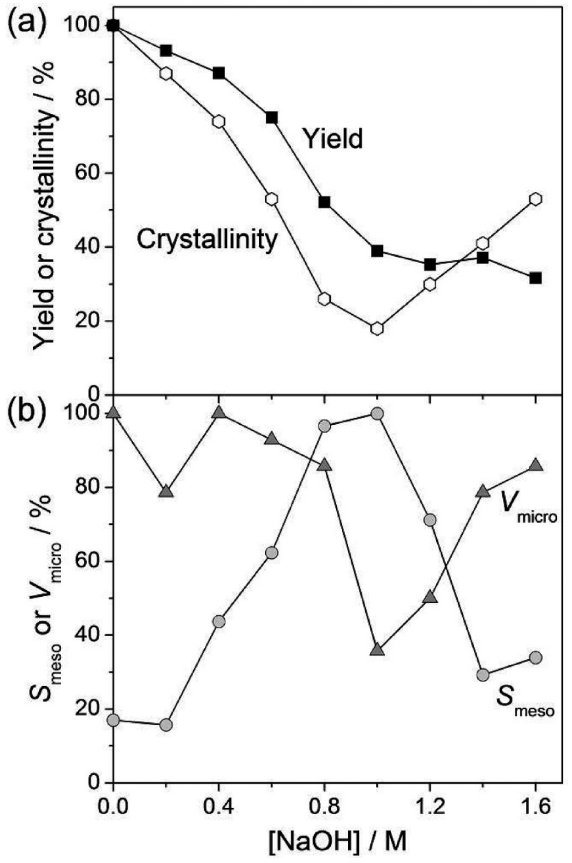

Figure 5. Influence of NaOH concentration on yield and crystallinity (a) and on micro- and mesoporosity (b) of alkaline-treated Z15. The parent zeolite is represented at 0 M.

Table 1. Chemical Composition of Selected Zeolites and Filtrates Obtained by Alkaline and Acid Treatments of Z15

sample	Si/Al[a] (mol mol^{-1})	Si/Al$_{filtrate}$[a] (mol mol^{-1})
P	15	–
1.0NaOH	3	89
1.4NaOH	3	–
1.0NaOH–0.1HCl	15	–

[a] Atomic absorption spectroscopy.

147 m^2 g^{-1} (0.6NaOH) and 236 m^2 g^{-1} (1.0NaOH). On the other hand, reduced uptakes at lowest relative pressures relate to lower micropore volumes. For example, the micropore volume of 0.6NaOH dropped slightly to 0.13 cm^3 g^{-1}, whereas for 1.0NaOH a V_{micro} = 0.05 cm^3 g^{-1} was obtained. More pronounced reductions in micropore volume (down to 0.02 cm^3 g^{-1}) were observed on treatment of Z10 (Table SI1). For Z15, treatment at 1.4 M NaOH resulted in a rather limited S_{meso} (69 m^2 g^{-1}), whereas V_{micro} was reduced to 0.11 cm^3 g^{-1}.

The mesopore size distribution of sample 0.6NaOH revealed the presence of contributions centered roughly near 3 and 35 nm (inset in Figure 1b). More severe alkaline treatment led to the presence of mesopores near 8 nm (1.0NaOH), while no clear preferential mesopore size was evidenced at even higher concentration (1.4NaOH). Intracrystalline mesopores were clearly visible in the TEM micrographs of 0.6NaOH and 1.0NaOH (Figure 4).

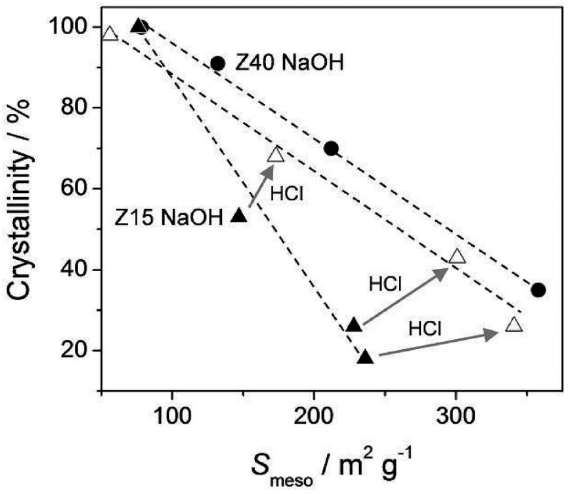

Figure 6. Influence of mesoporosity on crystallinity of treated Z15 (triangles) and Z40 (circles) zeolites. The solid symbols represent alkaline-treated samples (NaOH concentrations <1 M), and the open triangles represented the influence of a sequential acid treatment (0.1 M HCl).

For sample 0.6NaOH, lattice fringes were evident throughout the crystals and no evidence of zeolite amorphization was observed. More significant morphological changes were present in 1.0NaOH and 1.4NaOH, which should be related to the higher amount of Al-rich debris present in these samples (vide infra). In agreement with the nitrogen adsorption, fewer intracrystalline mesopores were evidenced observed in 1.4NaOH.

Figure 5 shows the development of S_{meso}, V_{micro}, and crystallinity with NaOH concentration in more detail. Up to 1.0 M NaOH the obtained solids displayed a gradually increasing mesopore surface area up to their maximum value, i.e., 100% or 236 m^2 g^{-1}. Conversely, at higher concentrations (1.2–1.8 M) a steep decrease down to ca. 30% was observed. The variation of microporosity showed an almost inverse relationship, decreasing down to ca. 35% at 1.0 M NaOH and then restoring to up to 80% at higher molarities. Crystallinity displayed a similar trend, decreasing strongly up to 1.0 M NaOH (down to ca. 20%) after which it rose up to ca. 50% (selected XRD patterns are presented in Figure SI2). It seems that two regimes of dissolution take place in the case of Z15, of which 1.0 M is the turning point. At concentrations <1.0 M, a selective dissolution occurs resulting in the formation of mesopores and a consequential reduction of crystallinity. At concentrations >1.0 M the dissolution appears to be less selective, resulting in a dissolution process similar to that of standard alkaline treatment on silicalite-1.[30] Hence, the resulting samples comprise a lower S_{meso} and a relatively high crystallinity.

The reduction of crystallinity upon the introduction of mesoporosity by desilication was thus far mostly semiquantitatively reported.[12,14,18] Figure 6 plots the crystallinities of alkaline-treated Z15 and Z40 as a function of their corresponding mesopore surface areas. For both zeolites linear regressions were obtained. For Z15 the crystallinity decreased with about 0.5% per m^2 g^{-1} of external surface, where as for Z40 this value was roughly 0.25% per m^2 g^{-1}.

^{27}Al and ^{29}Si MAS NMR was performed to investigate the influence of the alkaline treatments on the coordination of the Al and Si, respectively. As mentioned, ^{27}Al MAS NMR showed that

the parent Z15 comprised mostly framework Al, as well as a minor amount of extra-framework Al. Upon alkaline treatment the band attributed to framework Al (at 59 ppm) broadened, whereas the minor contribution related to extra-framework Al (at 0 ppm) was no longer distinguishable (Figure 7). We have recently demonstrated that the band at 59 ppm can be attributed to both purely framework and (partially) reintegrated Al.[30] It is therefore likely that, upon alkaline treatment, both the Al extracted from the zeolite framework to form a mesopore as well as the aluminum coordinated octahedrally in the parent (at 0 ppm) are partially reintegrated in the framework. The broadening of the band at 59 ppm should consequently be due to the copresence of purely framework and (partially) reintegrated Al. Likely, the more pronounced broadening of this band for 1.0NaOH compared to 1.4NaOH should be due to a greater heterogeneity of aluminum sites implied by the higher mesoporosity in the former sample. ^{29}Si MAS NMR performed on both the parent and treated samples revealed the presence of mostly crystalline (Q_4) components with chemical shifts centered around −112 ppm. Upon desilication, the components near −106 ppm increased, reflecting the higher Al content in the zeolite (Figure SI3). However, no major amorphization, as for example can occur upon alkaline treatment of FAU,[17] was evidenced.

Removal of Al-Rich Debris by Acid Treatment. Previous work has shown that relatively mild acid treatments can be used to selectively remove Al-rich debris from alkaline-treated zeolites.[18,28,41]

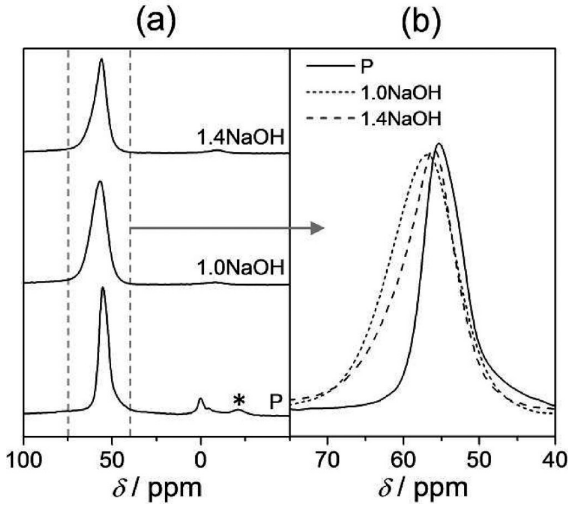

Figure 7. ^{27}Al MAS NMR of parent and alkaline-treated Z15 zeolites. The asterisk marks a spinning sideband.

More specifically, for ZSM-5 zeolites within the optimal Si/Al ratio (47), such treatment enabled restoration of the Si/Al ratio to that of the parent zeolite and a significant reduction of the Lewis acidity, while crystallinity and porosity remained mostly unaffected.[28] In the case of alkaline treatment of high-alumina ZSM-5 (Si/Al < 20), a noticeable influence on crystallinity and porosity is more likely since the amount of Al-rich debris is higher. We performed subsequent acid treatments to assess the influence of the latter species.

Table 2 presents four matrices in which the influence of an additional acid wash (0.02, 0.05, and 0.1 M HCl) on the yield, crystallinity, V_{micro}, and S_{meso} is summarized. Acid treatments of the parent zeolite resulted in high yields and little alteration of the porosity or crystallinity, attending to the high resistance of the MFI structure in acid media.[42] Conversely, the washing of the alkaline-treated zeolites resulted in a greater modification of their properties. The yields decreased with increasing severity of the acid treatment and the preceding alkaline treatment. This is unsurprising, since the amount of Al-rich debris typically increases with the severity of the alkaline treatment.[14,35] For example, sample 0.6NaOH (75% yield) showed a 9% weight loss upon treatment with 0.1 M HCl (0.6NaOH−0.1HCl, 68% yield). On the other hand, going from 1.0NaOH (39% yield) to 1.0NaOH−0.1HCl (28% yield) a drop of 28% was observed. Elemental analysis revealed that sample 1.0NaOH−0.1HCl exhibits a Si/Al ratio similar (15) to the parent zeolite (Table 1), which implies the removal of predominately Al-containing species. ^{29}Si MAS NMR confirmed the removal of these species, evidencing a substantially increased similarity between the sequentially treated sample and the parent zeolite (Figure SI3).

Upon acid washing, the crystallinity increased substantially. In fact, Figure 6 shows a significantly different linear relation due to the increase in both crystallinity and mesoporosity (vide infra). The corresponding slope is halved to −0.25% per $m^2\ g^{-1}$ and is similar to the crystallinity loss for alkaline-treated Z40. This clearly illustrates that upon alkaline treatment of low Si/Al ratio zeolites, the loss of crystallinity should be ascribed to (i) the introduction of mesopores and (ii) the presence of amorphous Al-rich debris.

The N_2 isotherms derived from the alkaline and acid-treated samples revealed the detrimental influence of the formed Al-rich debris on the porous properties. Figures 1b, c show increased uptakes at both low and middle-to-high relative pressures, which is reflected in gradual increases in V_{micro} and S_{meso}, respectively (Table 2). The external mesopore area of 0.6NaOH−0.1HCl increased from 147 $m^2\ g^{-1}$ (0.6NaOH) to 173 $m^2\ g^{-1}$, whereas the V_{micro} increased from 0.13 $cm^3\ g^{-1}$ (0.6 NaOH) to 0.16 $cm^3\ g^{-1}$. Even more significant was the change for 1.0NaOH: S_{meso} rose

Table 2. Yield, Crystallinity, and Porosity of Alkaline and Acid-Treated Z15 Zeolites

	yield (%)				crystallinity (%)				V_{micro} ($cm^3\ g^{-1}$)				S_{meso} ($m^2\ g^{-1}$)			
	HCl (M)															
NaOH (M)	0	0.02	0.05	0.1	0	0.02	0.05	0.1	0	0.02	0.05	0.1	0	0.02	0.05	0.1
0	100	99	100	100	100	96	97	98	0.14	0.15	0.16	0.16	76	70	58	56
0.6	75	75	74	68	53	60	61	68	0.13	0.15	0.16	0.16	147	158	160	173
0.8	52	51	47	43	26	30	44	43	0.12	0.14	0.14	0.15	228	273	299	301
1.0	39	38	34	28	18	24	24	26	0.05	0.08	0.11	0.14	236	240	288	341
1.4	37	–	–	27	41	–	–	56	0.11	–	–	0.14	69	–	–	137

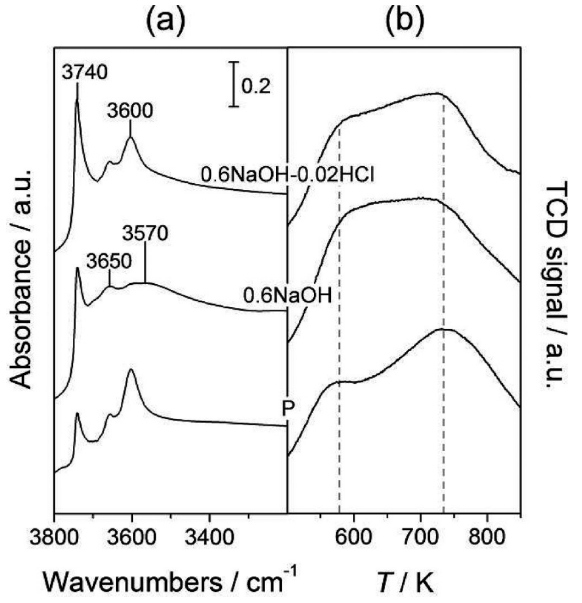

Figure 8. Infrared spectra in the OH stretching region (a) and NH_3-TPD profiles (b) of parent and treated Z15 zeolites.

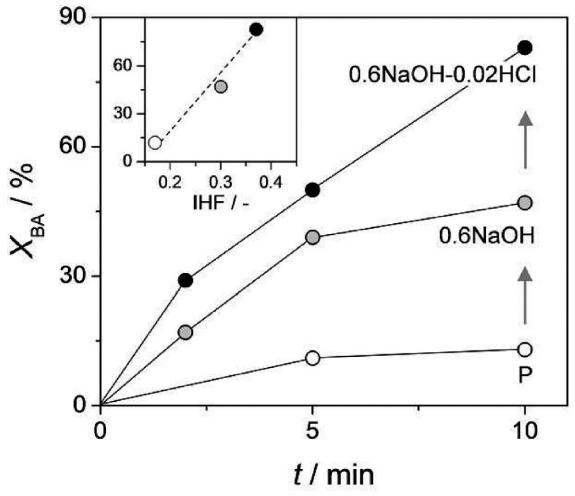

Figure 9. Conversion of benzyl alcohol (BA) over parent and treated Z15 zeolites in alkylation of toluene (T) with benzyl alcohol. Conditions: T/BA = 80, T = 433 K, and P = 0.5 MPa. The inset relates the conversion of benzyl alcohol at t = 10 min to the indexed hierarchy factor of each zeolite.

from 236 $m^2\ g^{-1}$ (1.0NaOH) to 341 $m^2\ g^{-1}$ (1.0NaOH−0.1HCl), and V_{micro} increased from 0.05 $cm^3\ g^{-1}$ (1.0NaOH) to 0.14 $cm^3\ g^{-1}$ (1.0NaOH−0.1HCl). Similar trends were observed upon acid treatment of alkaline-treated Z10 (to yield 1.2NaOH−0.1HCl, Figure 1a). In the latter case, an increase of the external surface (from 163 to 275 $m^2\ g^{-1}$) proved that alkaline treatment is also effective for MFI zeolites comprising very low Si/Al ratios. Moreover, this implies that the presence of substantial extra-framework aluminum in the parent zeolite does not inhibit the introduction of mesoporosity by desilication.

Inspection of the BJH mesopore size distribution associated with the treated Z15 zeolites confirmed that the mesoporosity of 0.6NaOH−0.1HCl remained mostly unaffected. On the other hand, for 1.0NaOH−0.1HCl, the intensity of the contributions around 8 nm increased substantially, attending to the large increase in mesoporosity. TEM shows that zeolites treated at 0.6MNaOH did not display significant differences prior to and after HCl washing. Conversely, for zeolite 1.0NaOH−0.1HCl the crystallites appeared to be more transparent to the electron beam, with sharper edge definition (Figure 4). This indicates that the Al-rich debris are only noticeable (by TEM) at high relative abundance.

With the substantial increase of V_{micro} and S_{meso}, and the reduced yield after acid treatment, our analyses using descriptors required refinement. For example, the indexed hierarchy factor increased from 0.30 (0.6NaOH) and 0.18 (1.0NaOH) to 0.43 (0.6NaOH−0.1HCl) and 0.74 (1.0NaOH−0.1HCl), respectively (Table SI1). The latter exceeded the highest value obtained for alkaline-treated Z40 (IHF = 0.69). The positive influence on the desilication efficiency was less obvious since, although S_{meso} increased, yields decreased. For Z15, when the increased external surface areas and the lower yields were taken into account (after 0.1 M HCl treatment, Table 2), the desilication efficiency increased by one-third (ca. 1 $m^2\ g^{-1}\ \%^{-1}$) to over 4 $m^2\ g^{-1}\ \%^{-1}$. In the case of Z10, the desilication efficiency doubled to 2 $m^2\ g^{-1}\ \%^{-1}$. As mentioned previously, the introduction of extensive intracrystalline mesoporosity in silicalite-1 was achieved by including external pore-direction agents (e.g., $Al(OH)_4^-$) in the alkaline solution.[30] The resulting hierarchical silicalite-1 (Z1000 in Figure 3) comprised a similar porosity compared to alkaline-treated ZSM-5 with Si/Al ratio within the optimal range (S_{meso} > 200 $m^2\ g^{-1}$). Moreover, the yield increased, implying concomitantly a comparable desilication efficiency of ca. 5 $m^2\ g^{-1}\ \%^{-1}$. Consequently, as is illustrated in Figure 3b, the efficiency of desilication can be increased by either sequential alkaline-acid treatment (in the case of Al-rich zeolites) or by the use of external PDA (in the case of all-silica zeolites).

Acid Properties and Catalytic Evaluation. To investigate the functionality of the parent and hierarchical zeolites, we have examined the acidity and catalytic performance of selected Al-rich (Z15) samples. The acidity of the parent and treated zeolites was studied by NH_3-TPD and infrared spectroscopy in the OH stretching region. Figure 8a reveals three principal absorbance bands in the IR spectrum of the parent zeolite. The most intense band, present around 3600 cm^{-1}, relates to the Brønsted acid sites. The band at 3740 cm^{-1}, which arises from isolated terminal silanols, was of substantial intensity due to the considerable external surface present in the parent sample. The weaker band at 3650 cm^{-1} could be related to extra- or partial framework aluminum,[19] consistent with ^{27}Al MAS NMR. Figure 8b shows the NH_3-TPD profiles of the parent and treated zeolites. Sample P comprised mostly strong acid sites, showing the typical desorption peak around 750 K. Additionally, a shoulder around 570 K is evidenced which should be attributed to Lewis acidity related to extra-framework aluminum.[19]

Upon alkaline treatment, the band at 3740 cm^{-1} in the IR spectrum of sample 0.6NaOH increased, attending to the higher external surface. However, the intensity was not as pronounced as previously reported for mesoporous Z40 prepared by desilication.[19] In addition, the band at 3600 cm^{-1}, related to Brønsted acid sites, was no longer clearly distinguishable: instead a broad band around 3570 cm^{-1} presented. Contributions in this region are typically associated with hydrogen bonding between neighboring hydroxyl groups, e.g., at defect sites, within the zeolite structure. These likely originate from the deposited Al-rich debris.[18,41] The contribution at 3650 cm^{-1}, although slightly

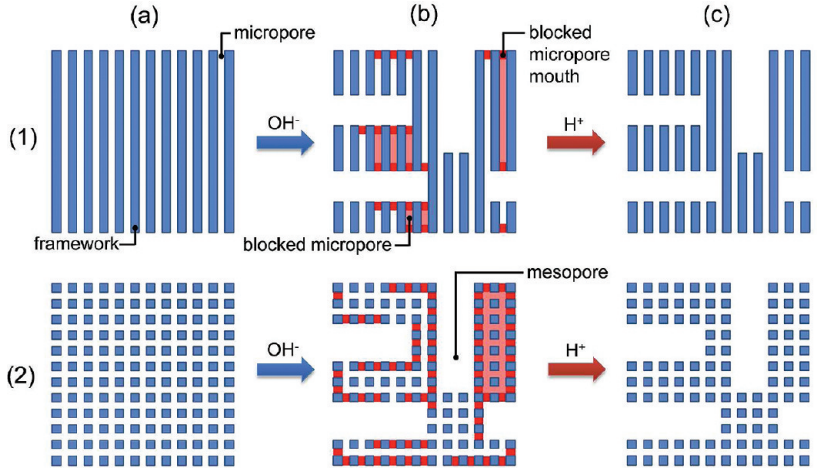

Figure 10. Schematic representation of the influence of the dimensionality and Si/Al ratio on the micropore blockage by Al-rich debris on the external surface upon sequential alkaline and acid treatment.

broadened, remained present. As no evidence of octahedrally coordinated Al was observed in the alkaline-treated zeolites by ^{27}Al MAS NMR, this demonstrates that the band at 3650 cm^{-1} can arise from hydroxyls associated with tetrahedrally coordinated Al species. The NH_3-TPD profile of the alkaline-treated sample 0.6NaOH displayed a similar contribution around 750 K compared to the parent, which proves that, although not evident in the IR spectrum of 0.6NaOH, the strong (Brønsted) acidity was preserved. In addition, a more pronounced shoulder can be observed around 570 K, attending to the increase in Lewis acidity due to the Al-rich deposits.[30] Quantification of the total acidity by integration shows that 0.6 NaOH comprises a total acidity 1.3 times higher than that of the parent zeolite.

After subsequent acid washing (sample 0.6NaOH−0.02HCl), the intensity of the band at 3740 cm^{-1} increased, the contribution related to Brønsted acid sites at 3600 cm^{-1} largely restored, and the broad band at 3570 cm^{-1} was no longer discernible. It is therefore likely that the Al-debris in 0.6NaOH masked some of the contributions in the OH stretching region of the infrared spectrum. The NH_3-TPD profile evidenced that the contribution around 570 K was significantly lower, whereas the peak related to the intrinsic Brønsted acidity (at 750 K) was mostly preserved. The removal of Al from the sample is corroborated by the reduction of the total acidity from 1.3 to approximately 1.1 times that of the parent zeolite. These results, combined with those from elemental analysis, confirm the restoration of the acid properties upon removal of the Al-rich debris by the acid-washing step.

The catalytic activity of P, 0.6NaOH, and 0.6NaOH−0.02HCl zeolites was examined in the alkylation of toluene with benzyl alcohol (Figure 9). The alkaline-treated sample (0.6NaOH) displayed a conversion of benzyl alcohol (X_{BA}) around three times higher compared to the parent zeolite (averaging X_{BA}'s at t = 5 and t = 10 min). The improved performance should be related to the introduced mesoporosity, increasing the accessibility of, and transport to, the active sites located in the micropores. The subsequent acid wash proved to be of great importance, enhancing the catalytic activity to over five times that of the parent, hereby evidencing a suppressing influence of the Al-rich debris on the activity. The inset in Figure 9 shows that the conversion of benzyl alcohol relates linearly to the IHFs. In the case of benzene alkylation with ethylene,[26] a similar trend was observed between the ethylbenzene productivity and the hierarchy factor of mesoporous Z40 prepared by desilication.

Clearly, in the preparation of the mesoporous low Si/Al ratio zeolites by desilication, it is essential to remove Al-rich debris by a sequential alkaline treatment. Similarly, it also proved that upon introduction of mesoporosity in unidirectional ZSM-22 zeolites (Si/Al = 42) by alkaline treatment the removal of these Al-rich species by a subsequent acid washing is highly beneficial.[18] Figure 10 schematically illustrates why, especially for zeolite crystals comprising a limited micropore dimensionality and/or a high Al content, the sequential acid treatment is of such paramount importance. Scenario 1a−c represents unidirectional microporous crystals of optimal Si/Al ratio (after ref 18), whereas scenario 2a−c represents 2D or 3D crystals that contain significantly more aluminum (this work). In both scenarios the alkaline treatment leads to the introduction of mesoporosity. However, the accessibility to the micropore volume is not optimal due to the deposition of Al-rich debris, blocking part of the micropore mouths. In the case of 1b this is implied by the high tendency of the unidirectional crystal to be blocked, whereas in 2b this is caused by the high Al content. In both cases, a subsequent acid wash (1c, 2c) is essential to remove the Al-rich debris and unblock the micropore mouths, hereby further increasing accessibility and restoring the micropore volume.

4. CONCLUSIONS

Full compositional flexibility in the preparation of mesoporous MFI zeolites by desilication was achieved. A systematic two-dimensional screening, as a function of the Si/Al ratio in the parent material and NaOH concentration, enabled assessment of the entire spectrum of solids than can be obtained by alkaline treatment. Desilication by NaOH alone proved effective in the Si/Al range of 12−200, and most efficient in the previously established range 25−50. The operational window of alkaline treatment is limited by the Al content of the parent zeolite: the absence of aluminum leads to the formation of mostly macropores, and an excess of aluminum results in blockage of micro- and mesopores by the formation of amorphous Al-rich deposits. Effective mesopore formation in these extremes can be attained

by either the addition of external pore-directing agent to the alkaline solution (all-silica zeolites) or the use of a sequential acid wash (Al-rich zeolites). The latter acid treatment not only uncovers full porosity; it also increases crystallinity and restores the Si/Al ratio and acidity. Catalytic evaluation in the alkylation of toluene with benzyl alcohol confirmed the superiority of the alkaline-treated (mesoporous) zeolites to the purely microporous parent. This is attributed to the improved access to the active sites located in the zeolite micropores. Moreover, the acid-washing step performed after desilication demonstrated to be essential, further enhancing the activity of the hierarchical zeolite. The desilication efficiency proved to be a powerful descriptor to evaluate the gain in mesoporosity with respect to the weight loss upon application of the post-synthetic treatments. The (indexed) hierarchy factor was highly useful in categorizing the obtained hierarchical structures and relating them to catalytic performance.

■ ASSOCIATED CONTENT

Supporting Information. Summary of characterization, additional MAS NMR spectra, and XRD patterns. This material is available free of charge via the Internet at http://pubs.acs.org.

■ AUTHOR INFORMATION

Corresponding Author
*Fax +41 44 633 14 05; e-mail jpr@chem.ethz.ch.

■ ACKNOWLEDGMENT

Financial support by ETH Zurich and the Swiss National Science Foundation (Project number 200021-134572) is acknowledged.

■ REFERENCES

(1) Pérez-Ramírez, J.; Christensen, C. H.; Egeblad, K.; Christensen, C. H.; Groen, J. C. *Chem. Soc. Rev.* **2008**, *37*, 2530.
(2) Schmidt, W. *ChemCatChem* **2009**, *1*, 53.
(3) Chal, R.; Gérardin, C.; Bulut, M.; van Donk, S. *ChemCatChem* **2011**, *3*, 67.
(4) Egeblad, K.; Christensen, C. H.; Kustova, M. Yu.; Christensen, C. H. *Chem. Mater.* **2008**, *20*, 946.
(5) Groen, J. C.; Peffer, L. A. A.; Moulijn, J. A.; Pérez-Ramírez, J. *J. Mater. Chem.* **2006**, *16*, 2121.
(6) Groen, J. C.; Moulijn, J. A.; Pérez-Ramírez, J. *Ind. Eng. Chem. Res.* **2007**, *46*, 4193.
(7) Groen, J. C.; Peffer, L. A. A.; Moulijn, J. A.; Pérez-Ramírez, J. *Microporous Mesoporous Mater.* **2004**, *69*, 29.
(8) Wei, X.; Smirniotis, P. G. *Microporous Mesoporous Mater.* **2006**, *97*, 97.
(9) Groen, J. C.; Sano, T.; Moulijn, J. A.; Pérez-Ramírez, J. *J. Catal.* **2007**, *251*, 21.
(10) Groen, J. C.; Abelló, S.; Villaescusa, L. A.; Pérez-Ramírez, J. *Microporous Mesoporous Mater.* **2008**, *114*, 93.
(11) Pérez-Ramírez, J.; Abelló, S.; Villaescusa, L. A.; Bonilla, A. *Angew. Chem., Int. Ed.* **2008**, *47*, 7913.
(12) Bonilla, A.; Baudouin, D.; Pérez-Ramírez, J. *J. Catal.* **2009**, *265*, 170.
(13) Mokrzycki, Ł.; Sulikowski, B.; Olejniczak, Z. *Catal. Lett.* **2009**, *127*, 296.
(14) Verboekend, D.; Groen, J. C.; Pérez-Ramírez, J. *Adv. Funct. Mater.* **2010**, *20*, 1441.
(15) Musilová-Pavlačková, Z.; Zones, S. I.; Čejka, J. *Top. Catal.* **2010**, *53*, 273.
(16) Sommer, L.; Mores, D.; Svelle, S.; Stöcker, M.; Weckhuysen, B. M.; Olsbye, U. *Microporous Mesoporous Mater.* **2010**, *132*, 384.
(17) de Jong, K. P.; Zečevič, J.; Friedrich, H.; de Jongh, P. E.; Bulut, M.; van Donk, S.; Kenmogne, R.; Finiels, A.; Hulea, V.; Fajula, F. *Angew. Chem., Int. Ed.* **2010**, *49*, 10074.
(18) Verboekend, D.; Chabaneix, A. M.; Thomas, K.; Gilson, J.-P.; Pérez-Ramírez, J. *CrystEngComm* **2011**, *13*, 3408.
(19) Groen, J. C.; Jansen, J. C.; Moulijn, J. A.; Pérez-Ramírez, J. *J. Phys. Chem. B* **2004**, *108*, 13062.
(20) Groen, J. C.; Peffer, L. A. A.; Moulijn, J. A.; Pérez-Ramírez, J. *Chem.—Eur. J.* **2005**, *11*, 4983.
(21) Groen, J. C.; Caicedo-Realpe, R.; Abelló, S.; Pérez-Ramírez, J. *Mater. Lett.* **2009**, *63*, 1037.
(22) Pérez-Ramírez, J.; Abelló, S.; Bonilla, A.; Groen, J. C. *Adv. Funct. Mater.* **2009**, *19*, 164.
(23) Abelló, S.; Pérez-Ramírez, J. *Phys. Chem. Chem. Phys.* **2009**, *11*, 2959.
(24) Abelló, S.; Bonilla, A.; Pérez-Ramírez, J. *Appl. Catal., A* **2009**, *364*, 191.
(25) Caicedo-Realpe, R.; Pérez-Ramírez, J. *Microporous Mesoporous Mater.* **2010**, *128*, 91.
(26) Pérez-Ramírez, J.; Verboekend, D.; Bonilla, A.; Abelló, S. *Adv. Funct. Mater.* **2009**, *19*, 3972.
(27) Groen, J. C.; Moulijn, J. A.; Pérez-Ramírez, J. *Microporous Mesoporous Mater.* **2005**, *87*, 153.
(28) Fernandez, C.; Stan, I.; Gilson, J.-P.; Thomas, K.; Vicente, A.; Bonilla, A.; Pérez-Ramírez, J. *Chem.—Eur. J.* **2010**, *16*, 6224.
(29) Thibault-Starzyk, F.; Stan, I.; Abelló, S.; Bonilla, A.; Thomas, K.; Fernandez, C.; Gilson, J.-P.; Pérez-Ramírez, J. *J. Catal.* **2009**, *264*, 11.
(30) Verboekend, D.; Pérez-Ramírez, J. *Chem.—Eur. J.* **2011**, *17*, 1137.
(31) Kustova, M. Yu.; Kustov, A. L.; Christensen, C. H. *Stud. Surf. Sci. Catal.* **2005**, *158*, 255.
(32) van Laak, A. N. C.; Safala, S. L.; Zečević, J.; Friedrich, H.; de Jongh, P. E.; de Jong, K. P. *J. Catal.* **2010**, *276*, 170.
(33) Gil, B.; Mokrzycki, Ł.; Sulikowski, B.; Olejniczak, Z.; Walas, S. *Catal. Today* **2010**, *152*, 24.
(34) Zhao, L.; Xu, C.; Gao, S. *J. Mater. Sci.* **2010**, *45*, 5406.
(35) van Miltenburg, A.; Pawlesa, J.; Bouzga, A. M.; Žilkova, N.; Čejka, J.; Stöcker, M. *Top Catal.* **2009**, *52*, 1190.
(36) Paixao, V.; Carvalho, A. P.; Rocha, J.; Fernandes, A.; Martins, A. *Microporous Mesoporous Mater.* **2010**, *131*, 350.
(37) Lippens, B. C.; de Boer, J. H. *J. Catal.* **1965**, *4*, 319.
(38) Brunauer, S.; Emmett, P. H.; Teller, E. *J. Am. Chem. Soc.* **1938**, *60*, 309.
(39) Barrett, E. P.; Joyner, L. G.; Halenda, P. P. *J. Am. Chem. Soc.* **1951**, *73*, 373.
(40) Čižmek, A.; Subotić, B.; Šmit, I.; Tonejc, A.; Aiello, R.; Crea, F.; Nastro, A. *Microporous Mater.* **1997**, *8*, 159.
(41) Verboekend, D.; Caicedo-Realpe, R.; Bonilla, A.; Santiago, M.; Pérez-Ramírez, J. *Chem. Mater.* **2010**, *22*, 4679.
(42) Oumi, Y.; Nemoto, S.; Nawata, S.; Fukushima, T.; Teranishi, T.; Sano, T. *Mater. Chem. Phys.* **2002**, *78*, 551.